WILEY VCH

RESEARCH ARTICLE

Unveiling the TADF Emitters with Apparent Negative Singlet-Triplet Gaps: Implications for Exciton Harvesting and OLED Performance

Xinrui Chen[a]#, Sergey Bagnich[g] #, Robert Pollice[b,c,h]#, Bing Li[a], Yuanyuan Zhu[a], Rishabh Saxena[g], Yixiao Yin[a], Weiguo Zhu[a], Alan Aspuru-Guzik*[b,c,d,e], Eli Zysman-Colman*[f], Anna Köhler*[g], Yafei Wang*[a]

[a] Jiangsu Collaborative Innovation Center of Photovoltaic Science and Engineering, Jiangsu Engineering Laboratory of Light-Electricity-Heat Energy-Converting Materials and Applications, School of Materials Science & Engineering, Changzhou University, Changzhou 213164, China. E-mail: qiji830404@hotmail.com

[b] Chemical Physics Theory Group, Department of Chemistry, University of Toronto, 80 St. George St, Toronto, Ontario M5S 3H6, Canada. E-mail: aspuru@utoronto.ca

[c] Department of Computer Science, University of Toronto, 40 St. George St, Ontario M5S 2E4, Canada

[d] Vector Institute for Artificial Intelligence, 661 University Ave Suite 710, Toronto, Ontario M5G 1M1, Canada

[e] Lebovic Fellow, Canadian Institute for Advanced Research (CIFAR), 661 University Ave, Toronto, Ontario M5G 1M1, Canada

[f] Organic Semiconductor Centre EaStCHEM School of Chemistry, Purdie Building, North Haugh University of St Andrews, St Andrews, Fife, UK KY16 9ST. E-mail: eli_journals@zysman-colman.com

[g] Soft Matter Optoelectronics, BIMF & BPI, University of Bayreuth, Universitätsstraße 30, 95447 Bayreuth, Germany. E-mail: anna.koehler@uni-bayreuth.de

[h] Current affiliation: Stratingh Institute for Chemistry, University of Groningen, Nijenborgh 4, Groningen, 9747 AG, The Netherlands.

Supporting information for this article is given via a link at the end of the document.

Abstract: Intramolecular through-space charge transfer thermally activated delayed fluorescence (TSCT-TADF) has attracted much attention recently as it can achieve both small energy splitting and high emission efficiency. However, the relationship of excited states between TSCT and through-bond charge transfer (TBCT) remains a challenge in the TSCT-TADF molecules. Herein, three compounds DPS-*m*-bAc, DPS-*p*-bAc and DPS-OAc that possess emissive TSCT and/or TBCT states were prepared. Interestingly, so-called inverted energy gap was found for both DPS-*m*-bAc and DPS-*p*-bAc in toluene solution, which results from the different charge transfer states of ICT_{high} and ICT_{low} proved by the detailed transient photoluminescence and calculated results. Intense emission from blue to yellow associated with high photoluminescence quantum yields of 70-100% were measured in doped polymethyl(methacrylate) (PMMA) films. Notably, compound DPS-*m*-bAc achieves the highest reverse intersystem crossing rate constant (k_{RISC}) of over 10^7 s^{-1} in PMMA film, benefiting from close-lying TSCT and TBCT states. The solution-processed device with DPS-*m*-bAc displays a maximum external quantum efficiency of 21.7%, and a relatively small efficiency roll-off (*EQE* of 20.2% @ 100 cd m^{-2}). Overall, this work demonstrates how with judicious emitter engineering, a synergy between different charge transfer excited states can be achieved, providing an avenue to achieve highly efficient solution-processed OLEDs.

Introduction

The efficient harvesting of non-emissive triplet excitons for light production in organic light-emitting diodes (OLEDs) remains a research theme of continuing interest.[1-4] Among the most successful designs are phosphorescent emitters,[5] which have been widely developed over the past two decades. By virtue of the presence of a heavy noble metal center, efficient intersystem crossing (ISC) between first excited singlet (S_1) and triplet (T_1) states occurs due to strong spin-orbit coupling (SOC) and these compounds efficiently emit light from the T_1 state.[6] However, the noble metals required in these emitters are scarce and so their use is not sustainable. Furthermore, (several) microseconds long triplet lifetime in phosphorescent emitters leads to a reduction of external quantum efficiency (EQE) at high current densities, the so-called efficiency roll-off effect, owing to bimolecular loss processes such as triplet-triplet annihilation and triplet-polaron quenching. An alternative class of emitters that can also achieve internal quantum efficiencies of up to 100% yet do not use scarce metal centers are purely organic thermally activated delayed fluorescence (TADF) compounds.[7-12] Whereas phosphorescent emitters collate all of the excitons on T_1 prior to emission via intersystem crossing (ISC) to harvest the singlet excitons, the excitons in TADF emitters emit only from the singlet state, this made possible by the endothermic up conversion of triplet excitons via reverse intersystem crossing (RISC) that is enabled by the small singlet-triplet energy gap (ΔE_{ST}) between the lowest-lying singlet and triplet excited states.[13] However, the RISC rate in organic TADF molecules is usually on the order of 10^5 to 10^6 s^{-1}.[14] This leads to a relatively long delayed fluorescence lifetime, which contributes to a large triplet exciton density in the TADF device and thus poor efficiency roll-off. Therefore, accelerating the RISC process is crucial to addressing this issue and improving device stability.

The RISC process within the regime of first order perturbation theory is described by the relationship $= \varkappa_{SO}/\Delta E_{ST}$,[15] where α is the first order mixing coefficient and $\varkappa_{SO}$ is the spin-orbit coupling value. Based on this, the development of small molecule TADF emitters relied robustly upon the minimization of ΔE_{ST}, which is

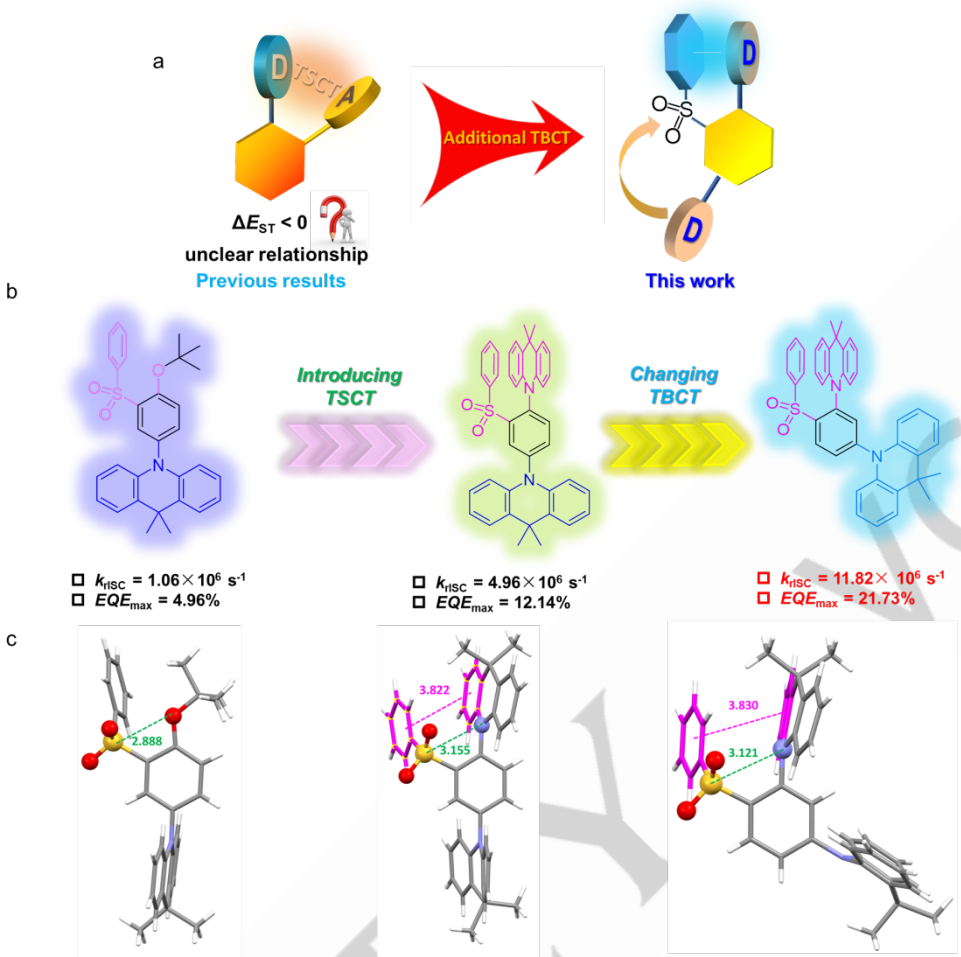

Figure 1. (a) Design strategy of organic emitters followed in this work; (b) structural evolutions of three molecules; (c) crystallographic data of three molecules

accomplished by reducing the spatial overlap of the highest occupied molecular orbital (HOMO) and the lowest unoccupied molecular orbital (LUMO).[10,16-17] So, an accurate measure of ΔE_{ST} is paramount to understanding the underlying RISC mechanism.

Most reported TADF molecules possess donor (D) and acceptor (A) moieties that are weakly coupled electronically by means of twisted conformations and possess emissive through-bond charge transfer (TBCT) excited states where the conjugation is mediated by a π-bonding network in the molecule.[9,18,19] There are examples of highly efficient TBCT-based TADF emitters with emission colors spanning from blue to red.[20-22] Despite the advances documented in these reports, a vast majority of these emitters possess k_{RISC} values slower than 10^6 s^{-1}, which contribute to poorer device performance, especially in terms of efficiency roll-off at high luminance. Through-space charge transfer (TSCT) emitters are compounds that contain weakly electronically coupled donor and acceptor motifs whose π-systems interact through space. Complicating the analysis of photophysics is that the contributions of through-space versus through-bond interaction are difficult to disentangle in a compound where donor and acceptor moieties are covalently linked. These compounds typically show fast k_{RISC},[23] which implies a small ΔE_{ST}. In the literature, there are now numerous reports of seemingly negative ΔE_{ST} values in some of these TSCT-based emitters (**Chart S1**).[24-30] The reduced internal conversion rate, a result of weak electronic coupling between the donor and acceptor moieties, leads to emission from higher lying states.[31-33] If this happens within the triplet manifold, it leads to a blue-shifted delayed luminescence spectrum (acquired with a millisecond time delay at 77 K) with respect to the steady-state emission spectrum (acquired at 77 K). This is often interpreted as a negative ΔE_{ST}; however, it must be noted that the parameter ΔE_{ST}, and in particular the associated notion of an inverted singlet-triplet gap, only has meaning if the orbitals involved describe the same electronic state yet differ in the spin states. In this manuscript we demonstrate that detailed low temperature (ca. 5 K) spectroscopic investigations, preferably time-resolved, are required to confidently identify the origin of the phosphorescence, and so the energy of the lowest-lying triplet state, and thus an accurate assignment of the ΔE_{ST} value. We illustrate how steady-state measurements conducted at 77 K can easily be misinterpreted to an erroneous assignment of ΔE_{ST}.

With the initial goal of designing fast k_{RISC} TSCT emitters for solution-processed OLEDs, we designed and synthesized molecules with a diphenyl sulfone (DPS) acceptor and 9,9-dimethyl-9,10-dihydroacridine (Ac) as the donor (**Figure 1c**). We realized that this family of compounds is ideally suited to address the issue of so-called negative singlet-triplet gap. There are two donors in DPS-*p*-bAc and DPS-*m*-bAc molecules where the □-systems are electronically coupled both through-bond and through-space, which leads to closely lying CT states. 77 K

steady-state emission from these CT states leads to the deceptive observation of a negative singlet-triplet gap. However, 5 K time-resolved measurements reveal the origins and energies of the singlet and triplet excited states and clarify that these compounds in fact have vanishingly small yet positive ΔE_{ST}. Intense emission from blue to green with high PLQY of 70-100% were observed in solution and film states. Notably, DPS-*m*-bAc shows the fastest k_{RISC} exceeding 10^7 s^{-1} in doped PMMA film. Solution-processed OLED based on DPS-*m*-bAc achieved a maximum EQE (EQE_{max}) of ~22% and a small efficiency roll-off, showcasing the value of this emitter design.

Results and Discussion

Synthesis and Characterization

As presented in **Scheme S1**, Ullmann coupling between the commercial thiophenol and either 2,4-difluoro-1-iodobenzene or 4-bromo-1-fluoro-2-iodobenzene generated the thioether derivatives 1 and 3, respectively. Oxidation with H_2O_2 afforded the corresponding sulfone derivatives 2 and 4. DPS-*m*-bAc was synthesized *via* double nucleophilic aromatic substitution from 2 and Ac in poor yield (16%). Similarly, DPS-*p*-bAc was prepared via a single nucleophilic aromatic substitution from 4 and Ac followed by Buchwald-Hartwig amination with another molecule of Ac in 74% yield. The Buchwald-Hartwig amination of compound 4 led to the unanticipated formation of DPS-OAc via nucleophilic attack of the base in moderate yield (63%). All three compounds were purified by column chromatography and recrystallization, and then fully characterized by ^{1}H NMR and ^{13}C NMR spectroscopy, MALDI-TOF mass spectrometry, HPLC (**Figure S1-S12**) and single-crystal X-ray diffraction. As illustrated in **Figure S13**, compounds DPS-*m*-bAc and DPS-*p*-bAc exhibit good thermal stability with decomposition temperatures (T_d) of 370 °C and 353 °C, respectively, at a 5% weight loss. By contrast, DPS-OAc has a lower T_d of only 241 °C, presumably due to the lability of the *tert*-butoxy group.

Single Crystal Analysis

Single crystals of all three emitters were obtained by slow evaporation of CH_2Cl_2/hexane (*v*/*v*=1:1) solutions of the respective compounds. The molecular packing in these crystals was investigated systematically, and all relevant data are listed in **Table S6**. As shown in **Figure S14**, donor and acceptor moieties are almost perfectly perpendicular with torsion angles in the range of 85-90°. Both DPS-*m*-bAc and DPS-*p*-bAc show cofacial arrangement between the acridan and diphenylsulfone (**Figure 1d**). There are some short intramolecular distances between the two cofacial fragments. For example, the ring-centroid/ring-centroid (one benzene ring in DPS and another one in the Ac moiety, see **Figure 1d**) distances were found to be 3.830 and 3.822 Å for compounds DPS-*m*-bAc and DPS-*p*-bAc, respectively. Also, the S/N distances are shorter than the sum of their van der Waals radii (ca. 3.4 Å). These short intramolecular distances demonstrate that through-space conjugation can occur in these two compounds.[34] Compared to DPS-*m*-bAc and DPS-*p*-bAc, no cofacial arrangement was found between the donor and acceptor moieties in DPS-OAc.

Electrochemical properties

Redox potentials of the three emitters were determined by cyclic voltammetry (CV) in dichloromethane using 0.1 M tetra-*n*-butylammonium hexafluorophosphate as the supporting electrolyte, and ferrocene/ferrocenium as the internal reference. Irreversible oxidation (E_{ox}) waves with onset potentials of 0.51, 0.50 and 0.47 V (vs. $E_{Fc/Fc+}$) were detected for DPS-*m*-bAc, DPS-*p*-bAc and DPS-OAc, respectively (**Figure S17**). The potentials for DPS-*m*-bAc and DPS-*p*-bAc are almost identical, suggesting that the positional isomerism only has a negligible effect on the oxidation potential. No reduction waves were detected within the electrochemical window of the solvent. Using the equation: E_{HOMO}

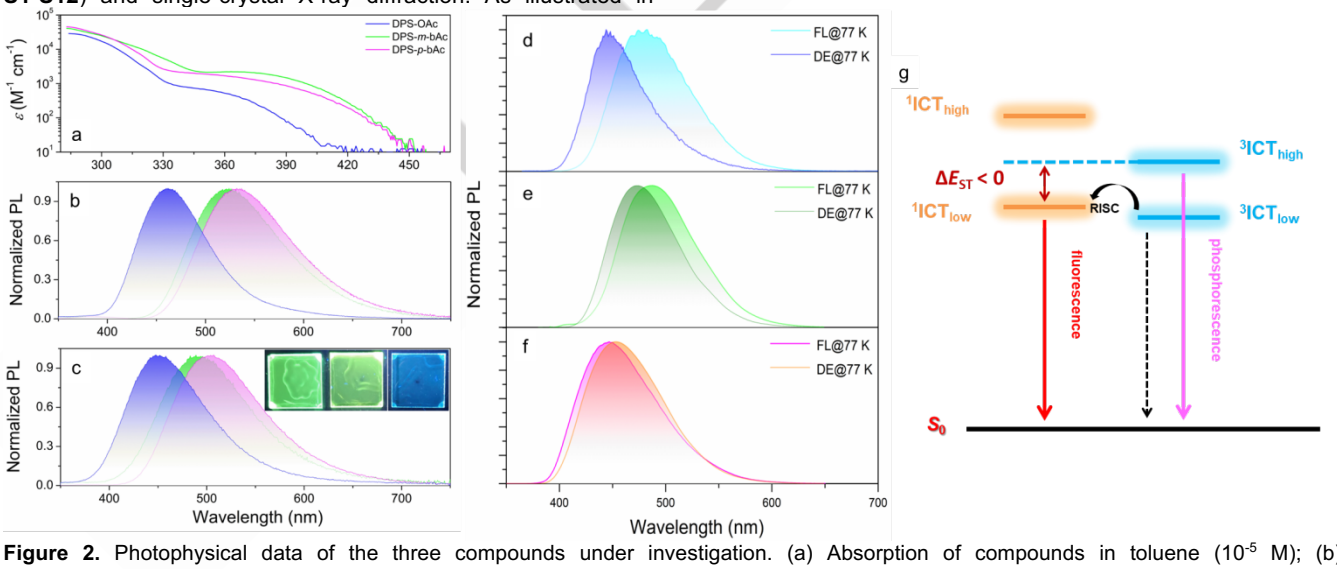

Figure 2. Photophysical data of the three compounds under investigation. (a) Absorption of compounds in toluene (10^{-5} M); (b) photoluminescence spectra of compounds (in toluene, λ_{exc} = 300 nm) at room temperature; (c) photoluminescence spectra of compounds (in 10 wt% PMMA, λ_{exc} = 300 nm) at room temperature (inset: the pictures from left to right are DPS-*m*-bAc, DPS-*p*-bAc and DPS-OAc); Low temperature (77 K) fluorescence (Fl) and delayed emission (DE, delayed with 1 ms) of compounds in toluene (d: DPS-*m*-bAc, e: DPS-*p*-bAc; f: DPS-OAc) with excitation wavelength of 300 nm; energy level diagram for the transitions observed in the solid solution of DPS-m-bAC.

= -(E^{ox}_{onset} + 4.8) eV, the HOMO energy levels of the emitters were calculated to be -5.31, -5.30, -5.27 eV for DPS-*m*-bAc, DPS-*p*-bAc and DPS-OAc, respectively. Based on the optical band (E^{opt}_{g}) gap, determined from the onset of absorption edge, and the calculated HOMO energy levels, the LUMO energy levels were evaluated to be -2.38, -2.39, -2.11 eV for DPS-*m*-bAc, DPS-*p*-bAc and DPS-OAc, respectively.

Photophysical Properties

The photophysical properties of the three compounds are summarized in **Table 1**. As seen in **Figure 2a** and **Figure S18**, all three compounds display two distinct absorption bands in toluene solution. The compound DPS-OAc possesses a strong absorption band centered at about 280 nm (4.43 eV), which we assign to the π-π* transitions localized on each of the donor and acceptor fragments, while the weak absorption band between 320 and 400 nm is associated with an intramolecular charge transfer (ICT) transition between the donor and acceptor fragments. The two compounds DPS-*m*-bAc and DPS-*p*-bAc show an increase in the intensity of the higher energy band, presumably due to the contribution from the localized π-π* transitions on the additional acridine. Furthermore, the lower energy band is much more intense and shifted to the red by about 25 nm (corresponding to about 0.2 eV in this energy range). Evidently, there is an additional charge-transfer contribution. A major difference between DPS-OAc and the other two compounds is the replacement of the *tert*-butoxy group with a second Ac moiety. In these two compounds, as demonstrated by the single crystal X-ray diffraction studies, there is a cofacial arrangement between the electron-rich acridan and the electron-deficient diphenylsulfone. We speculate that the additional contribution to the absorption spectrum is related to the additional Ac moiety and may possibly involve some through-space charge-transfer contribution. Thus, in addition to the ICT state already present in DPS-OAc, in DPS-*m*-bAc and DPS-*p*-bAc there exists another ICT state about 0.2 eV below it.

At room temperature, intense photoluminescence (PL) with peak maxima at 461, 524 and 532 nm (λ_{exc} = 300 nm) are observed in toluene for DPS-*m*-bAc, DPS-*p*-bAc and DPS-OAc, respectively (**Figure 2b**). The broad and structureless PL bands suggest that the emissions originate from ICT states. **Both the DPS-*m*-bAc and the DPS-*p*-bAc** emissions are red-shifted with respect to DPS-OAc, which is consistent with the trend observed in the absorption spectra, and is also consistent with emission from a ICT state in DPS-OAc whose origin is distinct from the ICT emissions of DPS-*m*-bAc and DPS-*p*-bAc; positive solvatochromism was observed in each of the three emitters, which corroborates the ICT character of the emissive excited states (**Figure S19**). The emission maximum red-shifts by 48 nm (0.20 eV) for DPS-*m*-bAc, 53 nm (0.22 eV) for DPS-*p*-bAc and 70 nm (0.28 eV) for DPS-OAc in CH_2Cl_2 relative to toluene, revealing decreasing CT character in these compounds in the order of DPS-OAc > DPS-*p*-bAc > DPS-*m*-bAc. In passing, we note that all three compounds show clear aggregation-induced emission enhancement (AIEE) in THF/H_2O mixtures with varying water fractions (f_w) (**Figure S20**).

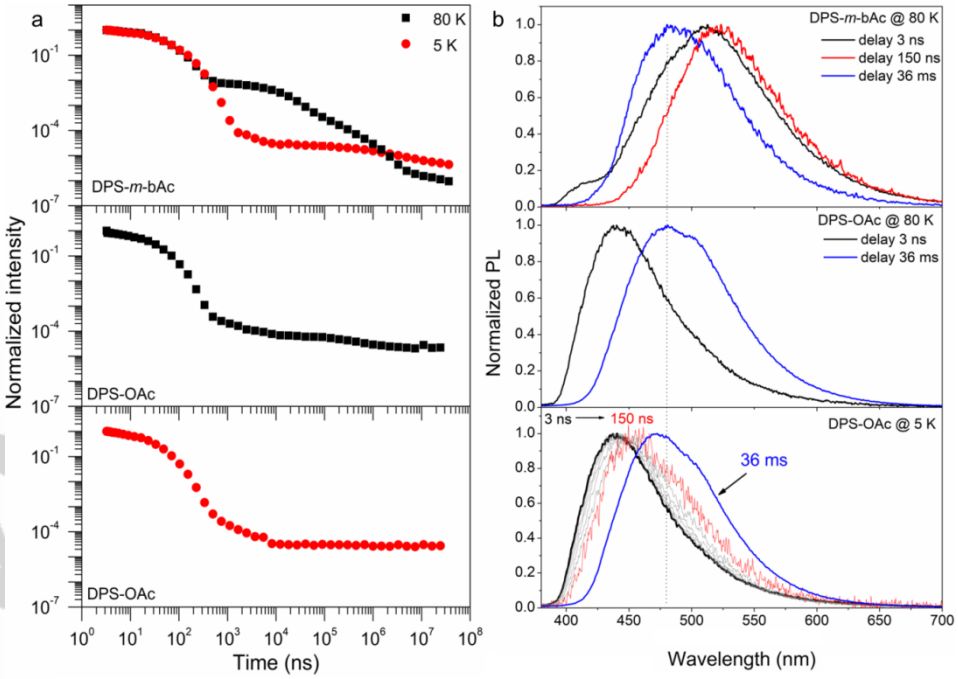

Figure 3. Photophysical data of the compounds in toluene. (a) Transient photoluminescence of the compounds in toluene solution at both 5 K and 80 K; (b) spectra taken at various delay times in a toluene glass of (top) DPS-*m*-bAc at 80 K, (middle) DPS-OAc at 80K, and (bottom) DPS-OAc at 5 K.

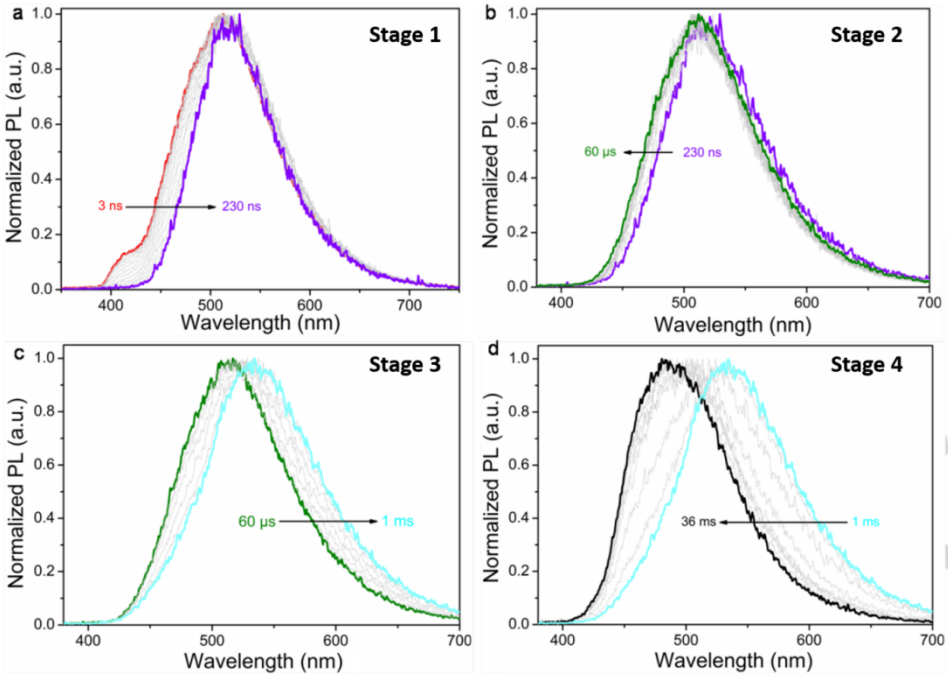

Figure 4. Spectra in toluene solution of DPS-*m*-bAc at 80 K and various time delays with (a-d) corresponding to the stages 1-4 indicated in **Figure 3a**.

The low-temperature (LT) emission was collected in toluene glass at (77 K) for steady state detection (FI) and for detection at 1 ms after excitation (DE), and is shown in **Figure 2d-f**. While for DPS-OAc, the long-lived component is slightly red-shifted from the steady-state emission, the opposite is the case for DPS-*p*-bAc and, in particular, for DPS-*m*-bAc. In these latter two compounds, the long-lived emission is shifted to the blue compared to the steady-state emission. When considering these data in isolation, it is tempting to attribute the long-lived emission to phosphorescence and the steady-state emission to fluorescence, and then to read off the presumed singlet and triplet energies from the onset of the emission bands. When doing so, one would arrive at the conclusion of a negative singlet-triplet gap, similar to some reported results of other TSCT TADF compounds shown in **Scheme 1**. The parameter ΔE_{ST} only has meaning if the singlet and triplet excited states reside on the same species. In an effort to account for the origins of the apparent inverted singlet-triplet gap, we undertook a detailed transient photoluminescence study. **Figure 2g** indicates the state ordering that we argue for in DPS-*m*-bAc (and also in DPS-*p*-bAc), based on the time-resolved luminescence data discussed in the next section.

Transient photoluminescence properties in toluene

In order to understand the origin of the unusual blue-shifted 77 K delayed emission spectra compared to the 77 K steady-state emission spectra presented in **Figure 2**, we investigated the time-resolved PL decays at both 5 and 80 K (**Figure 3** and **Figure S20**).

The transient decay of DPS-OAc in toluene at both temperatures consists of a short decay with about 50 ns lifetime, attributed to prompt fluorescence, and a very slowly decaying component that extends well into the regime of tens of ms, which must therefore be phosphorescence. The fluorescence red-shifts within 150 ns (**Figure 3b, bottom panel**), which is ascribed to the presence of different conformers in the toluene glass, each emitting at different energies and decaying with different kinetics. The phosphorescence spectrum, taken at 36 ms delay after the exciton pulse, does not change position with time (**Figure S22**), indicating a single low energy excited triplet state responsible for the emission. Since DPS-OAc does not have this lower energy ICT state (referred to as ICT_{low} henceforth) but only the higher energy ICT (ICT_{high}) state, these spectra serve as references for the $^1ICT_{high}$ and $^3ICT_{high}$ positions for all three compounds investigated here. When heating from 5 K to 80 K, we observe no significant change in the energies of these states (**Figure 3b, middle panel**).

For compound DPS-*m*-bAc the photophysical behavior is more complex. As with DPS-OAc, at 5 K the decay curve shows both prompt fluorescence and phosphorescence (**Figure 3a**). However, at 80 K, a new feature, assigned to TADF, strongly contributes to the total emission. We identify four distinct stages of the emission decay that are detailed in **Figure 4** and that are compared to DPS-OAc in **Figure 3b**.

The time range of stage 1 corresponds to the prompt fluorescence, the spectrum of which is shown in **Figure 4a**. We observe a high-energy band that decays faster than the main prompt fluorescence band. The position of this fast-decaying higher energy band coincides roughly with the energy of the $^1ICT_{high}$ observed in DPS-OAc, while the remaining prompt fluorescence band of DPS-*m*-bAc is further red-shifted. Thus, we attribute the initial emission centered at about 410 nm (3.02 eV) to the $^1ICT_{high}$ state, while the remaining emission, peaking at around 500 nm (2.48 eV), is assigned to an $^1ICT_{low}$ state at slightly lower energies, as indicated in **Figure 2g**.

Stage 2 (**Figure 4b**) corresponds to TADF, with a typical evolution of the delayed fluorescence spectra over time associated with some blue-shifting of the emission. This behavior can again be rationalized by the different RISC rates and associated delayed emission lifetimes of the different conformers present in the toluene glass.[35] Stage 3 reveals a red-shift of the

$^1ICT_{low}$ emission during the time from 60 □s to 1 ms (**Figure 4c**). Such behavior can be rationalized by assuming the presence of a lower energy conformer associated with a larger ΔE_{ST} and thus slower k_{RISC} (*vide infra* in quantum chemical calculations).

At the end of stage 3, there is a transition from delayed fluorescence to phosphorescence, as evident from the decay kinetics (**Figure 3a**). Stage 4 thus documents mainly the phosphorescence (**Figure 4d**) at times longer than 1 ms. We observe a blue-shift, which is unusual for phosphorescence spectra. Comparison between the 80 K spectra at 36 ms for DPS-*m*-bAc with DPS-OAc (**Figure 3b**) suggests that the species emitting after 36 ms is the $^3ICT_{high}$ state.

Figure **2g** provides an overview of the relative order of the excited states in DPS-*m*-bAc. In this compound, there is the same $^1ICT_{high}$ state that exists in DPS-OAc, yet there is also an additional $^1ICT_{low}$ state from the interaction between the acridine and the DPS moieties. The associated triplet state, $^3ICT_{low}$, is only about 0.2 eV lower in energy, which may be due to a rather small wavefunction overlap caused by the through-space contribution in this state or the larger through-bond delocalization obtained from the addition of the second acridine.[36] Even though the singlet-triplet splitting in the ICT_{high} state is larger than in the ICT_{low} state, the $^3ICT_{high}$ state is still at higher energy than the $^1ICT_{low}$ state. As a result, the 77 K spectra (**Figure 2a**) show a phosphorescence that occurs at higher energy than the fluorescence in the same compound, i.e., an "apparent negative singlet-triplet gap", yet the phosphorescence and the fluorescence pertain to states localized on different parts of the molecule. The photophysical behavior of DPS-*p*-bAc largely (**Figure S23**) is similar to that of DPS-*m*-bAc; however, there is a much smaller observed contribution from the emission from the ICT_{high} state.

We next explored whether this behavior is transferred into thin films, as this is relevant for device applications. We then considered the properties of our compounds when diluted at 10 wt% in both the electronically inert matrix PMMA (see Supporting Information) and the charge-transporting OLED relevant host mCP. The spectral and time-dependent features of the compounds remain preserved in both thin films (**Figure S24-S28**). Compared to the emission profiles in solution, small hypsochromic shifts are observed for all three emitters in the films (see **Figures 2b**, **c** and **S25**). The temperature-dependent transient PL decay curves reveal that the delayed components are gradually enhanced from 100 to 300 K (**Figure S27**). These results clearly demonstrate that the three compounds emit via TADF. The photophysical property in mCP are very similar to those in PMMA (**Table S1**). The transient PL decay curves still display clear double exponential decays under degassed conditions at room temperature, with a fast decay in the range of 26 ~ 34 ns, and a slower decay in the microsecond regime (2.7 ~ 7.0 μs, **Figure S28** and **Table 1**) for each of the three emitters. PLQYs of 95, 83 and 21% were measured for DPS-*m*-bAc, DPS-*p*-bAc and DPS-OAc in doped mCP host, respectively. The abnormally low emission efficiency of DPS-OAc in mCP is due to the energy transfer from the emission to the mCP host as the host has a lower triplet energy of 2.92 eV.

Based on the PLQY and emission lifetimes, the photophysical parameters for radiative decay (k_r), intersystem crossing (k_{ISC}) and reverse intersystem crossing (k_{RISC}) were calculated (using equations **S1** – **S6**[37]) and the relevant results are provided in **Table 1** and **Table S1**. Compared to DPS-OAc, both DPS-*m*-bAc and DPS-*p*-bAc exhibit much more delayed fluorescence and have a much higher k_{rISC} in both PMMA (**Table S1**) and mCP, ascribed to the presence of a second ITC state. Impressively, DPS-*m*-bAc shows the fastest k_{RISC} of all three

Photoluminescence properties in host-guest films

Table 1. Photophysical characterization of the three compounds studied in this work.

	DPS-*m*-bAc	DPS-*p*-bAc	DPS-OAc
[a] (λ_{abs}/ε)/(nm/10^5 L·mol^{-1}·cm^{-1})	283/0.68, 370/0.04	283/0.60, 362/0.02	283/1.17, 354/0.04
[a] λ_{em}/nm	524	532	461
[b] λ_{em} (77 K)/nm	480 (Fl), 445 (Ph)	486 (Fl), 472 (Ph)	447 (Fl), 453 (Ph)
[c] $^1ICT_{high}$ (80 K)/ nm (eV)	391 (3.17)	390 (3.17)	396 (3.13)
[c] $^3ICT_{high}$ (80 K)/ nm (eV)	425 (2.92)	430 (2.88)	417 (2.97)
[c] $^1ICT_{low}$ (5 K)/ nm (eV)	430 (2.88)	434 (2.86)	-
[c] $^3ICT_{low}$ (5 K)/ nm (eV)	432 (2.87)	437 (2.84)	-
[c] ΔE_{ST} (5 K)/eV	0.01	0.02	0.16
[d] λ_{em}/nm	506	515	4446
[d] τ_p/ns	26	32	34
[d] τ_d/μs	2.7	3.6	7.0
[d] Φ/%	95	83	21
[d] Φ_p/%	8.80	11.21	15.00
[d] Φ_d/%	86.20	71.79	6.00
[d] k_r/10^6 s^{-1}	3.1	3.4	/
[d] k_{nr}/10^5 s^{-1}	1.6	7.0	/
[d] k_{ISC}/10^7 s^{-1}	3.5	2.7	/
[d] k_{RISC}/10^7 s^{-1}	0.44	0.21	/
[e] E_{ox}/V	0.51	0.50	0.47
[f] E_{HOMO}/eV	-5.31	-5.30	-5.27
[f] E_{LUMO}/eV	-2.38	-2.39	-2.11
[f] E_g/eV	2.93	2.91	3.16

a: at the peak maximum in toluene solution at room temperature; b: at the peak maximum in toluene solution at 77 K; c: derived from the onset of time integrated fluorescent and phosphorescent spectra at 5 K for the lowest excited states; d: in a 10 wt% doped mCP film at room temperature; e: in CH_2Cl_2 solution at room temperature (*vs.* $E_{Fc/Fc+}$); f: E_{HOMO} = -(E_{ox}+4.8) eV, E_{LUMO} = (E_g + E_{HOMO}) eV, E_g = 1240/λ_{edge}.

compounds having values of 1.18 and 0.44 × 10^7 s^{-1} in PMMA and mCP, respectively, which are among the fastest RISC rate constants for TSCT-based emitters (**Figure S28d** and **Table S7**).

Computational studies

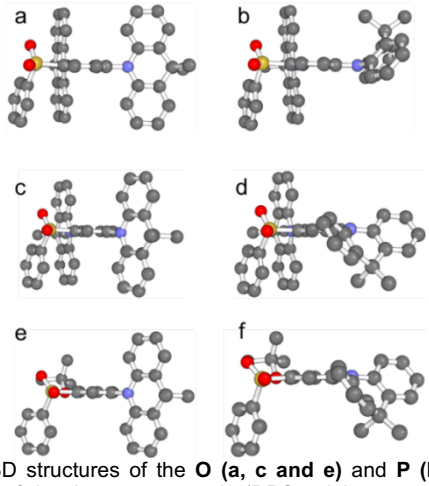

Figure 5. 3D structures of the **O (a, c and e)** and **P (b, d and f)** conformers of the three compounds (DPS-*m*-bAc: a and b; DPS-*p*-bAc: c and d; DPS-OAc: e and f) under study. The central benzene ring is observed from the side so that all its carbon atoms appear in one line. Hydrogen atoms are omitted for clarity.

From the spectroscopic studies, we have identified singlet and triplet emission from two different ICT states, that is ICT_{low} and ICT_{high}, remarkably without any intramolecular energy transfer between them. To rationalize the origin of these states, we turned to computations (see **Figures 5, 6** and VIII in Supporting Information). Importantly, we noted that the excited state parameters of the three compounds showed a significant conformational dependence. Acridan substituents attached via nitrogen to phenyl groups can either be orthogonal (referred to as **O** conformer, **Figure 5**) to the phenyl π-system, or parallel (referred to as **P** conformer, **Figure 5**). For both DPS-*m*-bAc and DPS-*p*-bAc, the two conformers are within 1 kcal/mol suggesting that both could be present in solution in significant amounts. For DPS-OAc, the **P** conformer is predicted to be almost 3 kcal/mol higher in energy which suggests it to be significantly less populated. Nevertheless, for all three compounds, the interconversion barriers between the **O** and **P** conformers are within 4 kcal/mol suggesting rapid interconversion.

Key simulated excited-state parameters of these conformers are summarized in **Table S2**. They show that the **O** conformers of DPS-*m*-bAc and DPS-*p*-bAc are predicted to have significantly smaller singlet-triplet gaps compared to the corresponding **P** conformers. In contrast, both the **O** and **P** conformers of DPS-OAc are predicted to have practically identical and large singlet-triplet gaps. Additionally, the **P** conformers generally show higher oscillator strengths for the vertical transitions between S_0 and S_1 across all three compounds, both in S_0 and in S_1 geometries, suggesting the **O** conformers to be less emissive than the **P** conformers. Furthermore, we find that the **P** conformers of DPS-*m*-bAc and DPS-*p*-bAc show significantly higher excitation energies between S_0 and S_1 compared to the corresponding **O** conformers. Notably, for DPS-OAc, the corresponding excitation energy for the **P** conformer is slightly lower than for the **O** conformer but they are similar.

Based on the computations, it would seem plausible that both prompt fluorescence and phosphorescence of DPS-OAc only take place from the **O** conformer, which is predicted to be lower in energy. However, as the first excited states in the **O** and **P** conformers of DPS-OAc are predicted to have similar energies, they cannot be distinguished and emission might also take place from the **P** conformer. This is consistent with the experimental

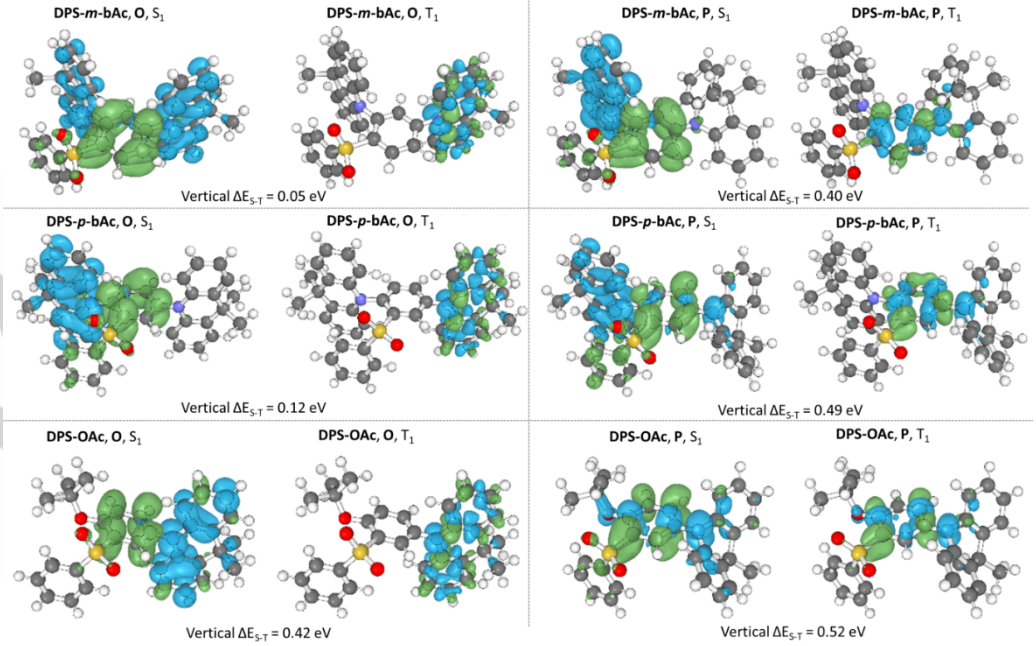

Figure 6. (d) Difference electron density plots for DPS-*m*-bAc, DPS-*p*-bAc and DPS-OAc in both their **O** and **P** conformers at the SOS-ωB88PP86 level of theory using r2SCAN-3c ground state geometries together with the corresponding vertical singlet-triplet gaps at the same level of theory.

observation of only one ICT_{high} state for that compound. Additionally, the computations also agree with the observed comparably large energy difference between fluorescence and phosphorescence and the absence of significant TADF for DPS-OAc as the corresponding singlet-triplet gap is predicted to be relatively large.

For both DPS-*m*-bAc and DPS-*p*-bAc, the computations suggest the potential involvement of both the **O** and the **P** conformers in their spectroscopic behavior. We noted in the experimental section that we observe a high-energy band decaying faster than the main prompt fluorescence band for DPS-*m*-bAc in stage 1. Additionally, we noted that this band coincides roughly with the fluorescence energy of the excited singlet state in DPS-OAc. In the simulations, we find that the S_1 state of the **P** conformer of DPS-*m*-bAc has significantly larger excitation energy than the S_1 state of the corresponding **O** conformer. The **P** conformer is also predicted to have a significantly higher oscillator strength and it has a comparable excitation energy as the S_1 state of the **O** conformer of **DPS-OAc**. Hence, the computations for DPS-*m*-bAc suggest that the S_1 state of the **P** conformer should show high-energy fluorescence, similar in energy to the DPS-OAc fluorescence, that decays faster than the S_1 state of the corresponding **O** conformer, and thus agrees qualitatively with the spectroscopic observations. Finally, the computations also correctly identify the high-energy fluorescent state with a large energy gap to the corresponding triplet state and the low-energy fluorescent state with a small singlet-triplet energy gap. Thus, based on our simulations, ICT_{low} would correspond to the excited states in the **O** conformer of DPS-*m*-bAc and DPS-*p*-bAc, and ICT_{high} would correspond to the excited states in the **P** conformer of these two compounds. For DPS-OAc, ICT_{high} could correspond to the excited states in either the **O** conformer or the **P** conformer.

However, agreement between simulation and experiment is not perfect as the excitation energies between S_0 and T_1 in the **P** conformers of both DPS-*m*-bAc and DPS-*p*-bAc are predicted to be lower in energy than between S_0 and S_1 in the corresponding **O** conformers. In our experiments, we observed part of the phosphorescence at a higher energy than the low-energy fluorescence. Moreover, the simulations systematically overestimate the excitation energies in these compounds as they are predicted to be in the UV region whereas our experiments show them to be in the VIS range which likely stems from both a neglect of excited state relaxation and a systematic misestimation of the excitation energies by the density functional approximation employed. Yet, systematic deviations in the simulated excitation energies obtained via density functional approximations are quite common. Additionally, the prediction of triplet excitation energies is expected to be less accurate than the corresponding singlet excitation energies with the computational methods used. Thus, overall, we suggest that the presence of both **O** and **P** conformers for the compounds under study, especially for DPS-*m*-bAc and DPS-*p*-bAc, can serve as a potential rationalization for the observed photoluminescence behavior. This model agrees well with the observations related to fluorescence, for which the computational methods are expected to deliver more accurate results, though there are some shortcomings in the

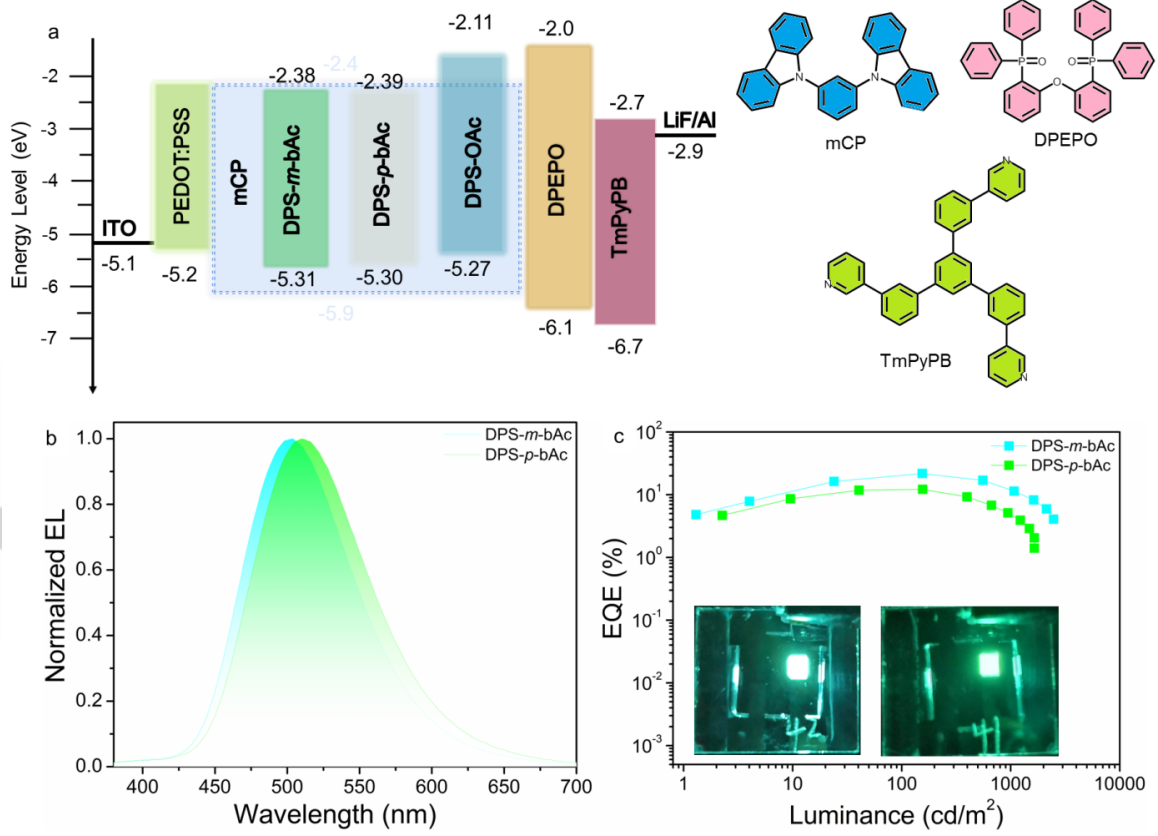

Figure 7. The energy levels, molecular structures in the device and devices performance. (a) energy levels of the device; (b) molecular structures; (c) EL spectra of the devices; (d) EQE-current density curves. Inset: the images of the devices (left is DPS-*m*-bAc, and right is DPS-*p*-bAc).

Table 2. Device performance with the three emitters.

Material	Dopant /wt %	V_{on} /V	L_{max} /cd m^{-2}	CE_{max} /cd A^{-1}	EQE_{max} /%	*EQE*/% (@100 cd m^{-2})	CIE (x, y)	λ_{EL} /nm
DPS-*m*-bAc	10%	4.0	2474	57.49	21.7	20.2	(0.22, 0.44)	504
DPS-*p*-bAc	10%	4.4	1649	34.77	12.1	11.5	(0.25, 0.49)	510
DPS-OAc	10%	4.4	117.3	7.11	5.0	0.6	(0.19, 0.23)	470

description of some observations related to phosphorescence. Importantly, however, the model is able to give a satisfactory explanation on why we can observe emission from $^3ICT_{high}$ at all. At first sight, emission from $^3ICT_{high}$ seems to violate Kasha's rule. There are two lower energy states available, that is $^3ICT_{low}$ and $^1ICT_{low}$, and in view of the small energy difference they have to $^3ICT_{high}$ one would expect them to be populated very efficiently through internal conversion or intersystem crossing, respectively. However, if the ICT_{high} pertains to the P conformer and ICT_{low} to the O conformer, this implies that these states are not on the same molecule but rather on different molecules in the solution or film. This readily accounts for the absence of energy transfer between ICT_{high} and ICT_{low}, and hence Kasha's rule is not violated.

To further characterize the excited states of the molecules computationally, we investigated the difference electron densities between the ground state (S_0) and the first electronic excited states (S_1 and T_1) in more detail (**Figure 6**). First, we observed across all three compounds that the lowest energy excited singlet states stem mainly from ICT excitations whereas the lowest energy excited triplet states stem largely from local excitations (LE). As expected, in the lowest energy excited singlet states, electron density is generally transferred from the donors (Ac) to the acceptor (DPS). Specifically, in the **O** conformer of DPS-*m*-bAc, both Ac groups donate electron density, in the corresponding **P** conformer only the Ac group ortho to the sulfone does. For DPS-*p*-bAc, we observe that in the **O** conformer only the Ac group ortho to the sulfone donates electron density, whereas in the **P** conformer both Ac groups do. For DPS-OAc, the Ac group donates electron density in both conformers but only the P conformer also shows contributions from the alkoxy group. Notably, the difference densities of the **O** and **P** conformers for DPS-*m*-bAc and DPS-*p*-bAc show comparable contributions of through-space interaction whereas the corresponding computed singlet-triplet gaps show a significant difference. This suggests that the contribution from the through-space charge transfer in these compounds has little to do with their singlet-triplet gaps.

We would like to emphasize that while the presence of multiple conformers can provide an explanation for the photophysical observations, we cannot rule out the involvement of higher-lying excited states. Based on additional computational investigations of higher excited singlet and triplet states, which are detailed in the Supporting Information, we find this explanation less likely.

Organic light-emitting diodes

To explore the device performance of these compounds, solution-processed OLEDs employing all three emitters as the dopant were fabricated with the configuration ITO/PEDOT:PSS (40nm)/mCP:dopant (10 wt%, 35 nm)/DPEPO (9 nm)/TmPyPB(45 nm)/LiF (0.5 nm)/Al (120 nm). In these devices, poly(3,4-ethylenedioxythiophene):poly(styrenesulfonic acid) (PEDOT:PSS) serves as the hole injection layer, while bis[2-(diphenylphosphino)phenyl] ether oxide (DPEPO) and 1,3,5-tri(m-pyrid-3-yl-phenyl)benzene (TmPyPB) act as the hole-blocking and electron-transport layers, respectively. The emitter layer consists of a 9,9'-(1,3-phenylene)bis-9*H*-carbazole (mCP) host blended with the dopant at an optimized doping level of 10 wt.%. The energy levels of the device as well as relevant molecular structures are depicted in **Figure 7a**.

The devices display intense electroluminescence (EL) with maxima, λ_{EL}, at 504, 510 and 470 nm for DPS-*m*-bAc, DPS-*p*-bAc and DPS-OAc, respectively (**Figure 7b** and **Figure S34a**). The broad and structureless EL profiles are similar to the PL spectra, indicating that the EL originates from the same excited state. The absence of host emission implies that a complete energy transfer occurs between the host and the dopant for DPS-*m*-bAc and DPS-*p*-bAc. For DPS-OAc, the broad emission at 400 nm could be assigned to originating from the host matrix. The corresponding CIE (Commission International de l'Éclairage) chromaticity coordinates are (0.22, 0.44), (0.25, 0.49) and (0.19, 0.23) for DPS-*m*-bAc, DPS-*p*-bAc and DPS-OAc, respectively (**Figure S35**). **Figure 7c** and **S34c** show the external quantum efficiency (η_{ext}) versus luminance and current density-voltage-luminance (*J*-*V*-*L*) curves. As indicated in **Table 2**, all devices display satisfying turn-on voltages (V_{on} in 1 cd m^{-2}) in the range of 4.0–4.4 V. Owing to the highest emission efficiency in the film, the DPS-*m*-bAc-based device exhibited the best performance with a maximum η_{ext} of 21.7%, which is among the best performances for the TSCT-type TADF solution-processed OLEDs with simple device structure (**Table S6**). Impressively, the device still possesses very high EQE of 20.2% at 100 cd m^{-2} (**Figure 7c**, Table 2), implying a relatively small efficiency roll-off. The DPS-*p*-bAc-based device shows a lower η_{ext} of 12.1% presumably due to its lower PLQY. As for DPS-OAc, the device shows a poor performance with an η_{ext} of 5.0%, accompanied by a severe efficiency roll-off, probably due to the poor stability of the *tert*-butoxy group. Notably, the unmatched energy levels between mCP and DPS-OAc is likely also responsible for the unsatisfying device performance.

Conclusion

In summary, we addressed the issue of why an apparent negative singlet-triplet gap can be observed in some emitters. For this purpose, three systematically tuned organic emitters, namely

DPS-*m*-bAc, DPS-*p*-bAc and DPS-OAc, were synthesized and fully characterized. All three compounds possessed clear TADF and AIEE properties. An analysis of the absorption spectra in solution reveals that while DPS-*m*-bAc and DPS-*p*-bAc possess two ICT states, namely, ICT_{high} and ICT_{low} states, DPS-OAc possesses only the ICT_{high} state and thus serves as a reference for the $^1ICT_{high}$ and $^3ICT_{high}$ energies. Time-resolved photoluminescence studies (performed at both 5 K and 80 K) indicate that $^3ICT_{low}$ and $^1ICT_{low}$ are nearly isoenergetic due to some through-space contribution to this ICT state while there is a relatively large gap between the $^1ICT_{high}$ and $^3ICT_{high}$ states due to the through-bond nature of this ICT state. Importantly, overall, the $^3ICT_{high}$ state lies higher in energy than both $^1ICT_{low}$ and $^3ICT_{low}$, and internal conversion between the higher and lower ^3ICT states is slower than phosphorescence from $^3ICT_{high}$. As a result, 77 K measurements show phosphorescence from $^3ICT_{high}$ in addition to the fluorescence from $^1ICT_{low}$, which could easily be misinterpreted as a negative singlet-triplet gap, even though, as clarified with the help of detailed time-resolved photoluminescence measurements performed at 5 K, all the compounds have very small yet positive singlet-triplet gaps. Solid-state photophysical investigations show that DPS-*m*-bAc shows the highest k_{RISC} with a value on the order of 10^7 s^{-1} due to its strong TSCT effect and a relatively weak TBCT effect. Correspondingly, the solution-processed OLEDs based on DPS-*m*-bAc achieved the highest EQE of 21.7%, concomitant with small efficiency roll-off.

Supporting Information

Supplemental Information can be found online or from the author. [CCDC 2109592, 2109595 and 2109596 contains the supplementary crystallographic data for this paper. These data can be obtained free of charge from The Cambridge Crystallographic Data Centre via www.ccdc.cam.ac.uk/data_request/cif.]

Acknowledgements

Financial support was from the National Natural Science Foundation of China (Nos. 51773021, 51911530197, 514 73140), Six talent peaks project in Jiangsu Province (XCL-102), Natural Science Fund for Colleges and Universities in Jiangsu Province (No. 19KJA430002). R.P. acknowledges funding through a Postdoc. Mobility fellowship by the Swiss National Science Foundation (SNSF, Project No. 191127). A. A.-G. thanks Dr. Anders G. Frøseth for his generous support. A. A.-G. also acknowledges the generous support of Natural Resources Canada and the Canada 150 Research Chairs program. In addition, this research was enabled in part by support provided by Compute Ontario (https://www.computeontario.ca/) and Compute Canada (www.computecanada.ca). AK, SB and RS acknowledge funding from the Deutsche Forschungsgemeinschaft (KO 3973/8-1) and through the EU HORIZON-MSCA-2021-DN TADF solutions, project number 101073045.

Keywords: thermally activated delayed fluorescence • charge transfer • delayed fluorescence • fast reverse intersystem crossing • solution-processed OLED

[1] H. Zhang, B. Zhang, Y. Zhang, Z. Xu, H. Wu, P.-A. Yin, Z. Wang, Z. Zhao, D. Ma, B. Z. Tang, *Adv. Funct. Mater.* **2020**, *30*, 2002323.

[2] Q. Wei, P. Kleine, Y. Karpov, X. Qiu, H. Komber, K. Sahre, A. Kiriy, R. Lygaitis, S. Lenk, S. Reineke, B. Voit, *Adv. Funct. Mater.* **2017**, *27*, 1605051.

[3] N. A. Kukhta, T. Matulaitis, D. Volyniuk, K. Ivaniuk, P. Turyk, P. Stakhira, J. V. Grazulevicius, A. P. Monkman, *J. Phys. Chem. Lett.* **2017**, *8*, 6199-6205.

[4] C.-H. Lin, Y.-Y. Chang, J.-Y. Hung, C.-Y. Lin, Y. Chi, M.-W. Chung, C.-L. Lin, P.-T. Chou, G.-H. Lee, C.-H. Chang, W.-C. Lin, *Angew. Chem. Int. Ed.* **2011**, *50*, 3182-3186.

[5] M. A. Baldo, D. F. O'Brien, Y. You, A. Shoustikov, S. Sibley, M. E. Thompson, S. R. Forrest, *Nature* **1998**, *395*, 151-154.

[6] J. Kalinowski, V. Fattori, M. Cocchi, J. A. G. Williams, *Coord. Chem. Rev.* **2011**, *255*, 2401-2425.

[7] K. Goushi, C. Adachi, *Appl. Phys. Lett.* **2012**, *101*, 023306.

[8] H. Uoyama, K. Goushi, K. Shizu, H. Nomura, C. Adachi, *Nature* **2012**, *492*, 234-238.

[9] J.-M. Teng, Y.-F. Wang, C.-F. Chen, *J. Mater. Chem. C* **2020**, *8*, 11340-11353.

[10] S. K. Jeon, H. L. Lee, K. S. Yook, J. Y. Lee, *Adv. Mater.* **2019**, *31*, 1803524.

[11] M. Y. Wong, E. Zysman-Colman, *Adv. Mater.* **2017**, *29*, 1605444.

[12] Y. Liu, C. Li, Z. Ren, S. Yan, M. R. Bryce, *Nat. Rev. Mater.* **2018**, *3*, 18020.

[13] H. Nakanotani, T. Higuchi, T. Furukawa, K. Masui, K. Morimoto, M. Numata, H. Tanaka, Y. Sagara, T. Yasuda, C. Adachi, *Nat. Commun.* **2014**, *5*, 4016.

[14] H. S. Kim, J. Y. Lee, S. Shin, W. Jeong, S. H. Lee, S. Kim, J. Lee, M. C. Suh, S. Yoo, *Adv. Funct. Mater.* **2021**, *31*, 2104646.

[15] H. Noda, X.-K. Chen, H. Nakanotani, T. Hosokai, M. Miyajima, N. Notsuka, Y. Kashima, J.-L. Brédas, C. Adachi, *Nat. Mater.* **2019**, *18*, 1084-1090.

[16] Y. Tao, K. Yuan, T. Chen, P. Xu, H. Li, R. Chen, C. Zheng, L. Zhang, W. Huang, *Adv. Mater.* **2014**, *26*, 7931-7958.

[17] Z. Yang, Z. Mao, Z. Xie, Y. Zhang, S. Liu, J. Zhao, J. Xu, Z. Chi, M. P. Aldred, *Chem. Soc. Rev.* **2017**, *46*, 915-1016.

[18] X.-K. Chen, D. Kim, J.-L. Brédas, *Acc. Chem. Res.* **2018**, *51*, 2215-2224.

[19] R. K. Konidena, J. Y. Lee, *Chem. Rec.* **2019**, *19*, 1499-1517.

[20] M. Yang, I. S. Park, T. Yasuda, *JACS* **2020**, *142*, 19468-19472.

[21] C.-M. Hsieh, T.-L. Wu, J. Jayakumar, Y.-C. Wang, C.-L. Ko, W.-Y. Hung, T.-C. Lin, H.-H. Wu, K.-H. Lin, C.-H. Lin, S. Hsieh, C.-H. Cheng, *ACS Appl. Mater. Interfaces* **2020**, *12*, 23199-23206.

[22] T.-A. Lin, T. Chatterjee, W.-L. Tsai, W.-K. Lee, M.-J. Wu, M. Jiao, K.-C. Pan, C.-L. Yi, C.-L. Chung, K.-T. Wong, C.-C. Wu, *Adv. Mater.* **2016**, *28*, 6976-6983.

[23] Y. Wada, H. Nakagawa, S. Matsumoto, Y. Wakisaka, H. Kaji, *Nat. Photonics* **2020**, *14*, 643-649.

[24] C. S. Oh, D. d. S. Pereira, S. H. Han, H.-J. Park, H. F. Higginbotham, A. P. Monkman, J. Y. Lee, *ACS Appl. Mater. Interfaces* **2018**, *10*, 35420-35429.

[25] L. Gan, Z. Xu, Z. Wang, B. Li, W. Li, X. Cai, K. Liu, Q. Liang, S.-J. Su, *Adv. Funct. Mater.* **2019**, *29*, 1808088.

[26] X. Tang, L.-S. Cui, H.-C. Li, A. J. Gillett, F. Auras, Y.-K. Qu, C. Zhong, S. T. E. Jones, Z.-Q. Jiang, R. H. Friend, L.-S. Liao, *Nat. Mater.* **2020**, *19*, 1332-1338.

[27] Y. Mei, D. Liu, J. Li, H. Li, W. Wei, *J. Mater. Chem. C* **2021**, *9*, 5885-5892.

[28] T. Huang, Q. Wang, S. Xiao, D. Zhang, Y. Zhang, C. Yin, D. Yang, D. Ma, Z. Wang, L. Duan, *Angew. Chem. Int. Ed.* **2021**, *60*, 23771-23776.

[29] H. L. Lee, K. H. Lee, J. Y. Lee, H. J. Lee, *J. Mater. Chem. C* **2021**, *9*, 7328-7335.

[30] C. Wu, W. Liu, K. Li, G. Cheng, J. Xiong, T. Teng, C.-M. Che, C. Yang, *Angew. Chem. Int. Ed.* **2021**, *60*, 3994-3998.

[31] F. Rodella, R. Saxena, S. Bagnich, D. Banevičius, G. Kreiza, S. Athanasopoulos, S. Juršėnas, K. Kazlauskas, A. Köhler, P. Strohriegl, *J. Mater. Chem. C* **2021**, *9*, 17471-17482.

[32] D. Sun, R. Saxena, X. Fan, S. Athanasopoulos, E. Duda, M. Zhang, S. Bagnich, X. Zhang, E. Zysman-Colman, A. Köhler, *Adv. Sci.* **2022**, *9*, 2201470.

[33] L. G. Franca, A. Danos, A. Monkman, *J. Phys. Chem. Lett.* **2023**, *14*, 2764-2771.

[34] L. Sicard, C. Quinton, F. Lucas, O. Jeannin, J. Rault-Berthelot, C. Poriel, *J. Phys. Chem. C* **2019**, *123*, 19094-19104.

[35] S. Kumar, L. G. Franca, K. Stavrou, E. Crovini, D. B. Cordes, A. M. Z. Slawin, A. P. Monkman, E. Zysman-Colman, *J. Phys. Chem. Lett.* **2021**, *12*, 2820-2830.

[36] E. L. Frankevich, A. A. Lymarev, I. Sokolik, F. E. Karasz, S. Blumstengel, R. H. Baughman, H. H. Hörhold, *Phys. Rev. B* **1992**, *46*, 9320-9324.

[37] F. B. Dias, T. J. Penfold, A. P. Monkman, *Method. Appl. Fluoresc.* **2017**, *5*, 012001.

WILEY VCH

Table of Contents

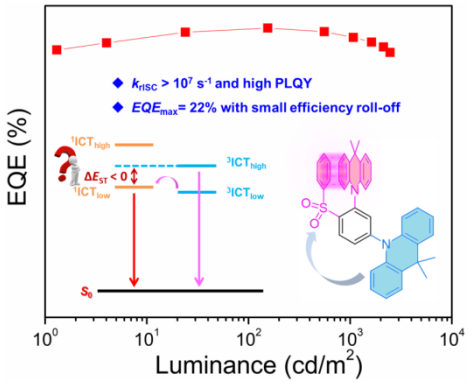

Three structurally related charge transfer-based compounds DPS-*m*-bAc, DPS-*p*-bAc and DPS-OAc were prepared. Notably, compound DPS-*m*-bAc shows the fastest reverse intersystem crossing rate constant of the three of over 10^7 s^{-1} in doped PMMA film as a result of the very small singlet-triplet gap. A maximum external quantum efficiency of 21.7% is achieved for the DPS-*m*-bAc-based solution-processed device.